

Human Respiratory Syncytial Virus Nucleoprotein and Inclusion Bodies Antagonize the Innate Immune Response Mediated by MDA5 and MAVS

Aaron W. Lifland,^a Jeenah Jung,^a Eric Alonas,^a Chiara Zurlo,^a James E. Crowe, Jr.,^b and Philip J. Santangelo^a

Wallace H. Coulter Department of Biomedical Engineering, Georgia Institute of Technology and Emory University, Atlanta, Georgia, USA,^a and Departments of Pediatrics and Pathology, Microbiology and Immunology, Vanderbilt University School of Medicine, Nashville, Tennessee, USA^b

Currently, the spatial distribution of human respiratory syncytial virus (hRSV) proteins and RNAs in infected cells is still under investigation, with many unanswered questions regarding the interaction of virus-induced structures and the innate immune system. Very few studies of hRSV have used subcellular imaging as a means to explore the changes in localization of retinoic-acid-inducible gene-I (RIG-I)-like receptors or the mitochondrial antiviral signaling (MAVS) protein, in response to the infection and formation of viral structures. In this investigation, we found that both RIG-I and melanoma differentiation-associated gene 5 (MDA5) colocalized with viral genomic RNA and the nucleoprotein (N) as early as 6 h postinfection (hpi). By 12 hpi, MDA5 and MAVS were observed within large viral inclusion bodies (IB). We used a proximity ligation assay (PLA) and determined that the N protein was in close proximity to MDA5 and MAVS in IBs throughout the course of the infection. Similar results were found with the transient coexpression of N and the phosphoprotein (P). Additionally, we demonstrated that the localization of MDA5 and MAVS in IBs inhibited the expression of interferon β mRNA 27-fold following Newcastle disease virus infection. From these data, we concluded that the N likely interacts with MDA5, is in close proximity to MAVS, and localizes these molecules within IBs in order to attenuate the interferon response. To our knowledge, this is the first report of a specific function for hRSV IBs and of the hRSV N protein as a modulator of the innate immune response.

Currently, the spatial biology of human respiratory syncytial virus (hRSV) is still under investigation, with many questions still unanswered about the ultrastructure of viral and host protein complexes in infected cells. To date, the function and complete composition of cytoplasmic inclusion bodies, as well as details of the host cell interactions with these virus-specific structures, are still unknown. Host cell interactions are accomplished through varied means, but first-line detectors of viral infections primarily involve two kinds of receptors: the cytoplasmic pattern recognition receptors, including the retinoic acid-inducible gene I (RIG-I) and melanoma differentiation-associated gene 5 (MDA5), both RNA helicases, and the pathogen-associated molecular pattern receptors, known as the Toll-like receptors (TLRs) (1, 18). TLR3 and TLR7 sense double- and single-stranded RNA, respectively, and in most cell types reside within endosomes (18). In contrast, TLR4, expressed on the cell surface, plays a role in sensing viral surface glycoproteins (18). RIG-I and MDA5 reside within the cytosol, and there are reports of them responding to both single- and double-stranded RNA (18). TLR signaling, mediated by MyD88, and RIG-I-like receptor signaling, mediated by the mitochondrial antiviral signaling (MAVS) protein (also known as the interferon promoter-stimulating factor 1 [IPS-1] adaptor protein), results in the production of interferon (18).

In response to hRSV, both TLRs and RIG-I-like receptors have been implicated in the general response to the infection. The hRSV fusion (F) protein has been shown to antagonize TLR4 in a mouse model (12). In A549 and mouse embryonic fibroblast (MEF) cells, it has been shown that RIG-I was essential for promoting the innate immune response, with MDA5 playing an auxiliary role (16, 17, 30). Even though there has been some confusion in the literature, recent results depicting the early events (0 to 6 h postinfection [hpi]) of an hRSV infection have shown that both

RIG-I and MDA5 play a significant role in both NF- κ B and IRF3 signaling (30).

In addition, a number of viral proteins have been implicated in decreasing the innate response to hRSV. The highly glycosylated attachment (G) protein has been shown to inhibit TLR3/4 signaling in dendritic cells. Nonstructural protein 1 (NS1) expression has been correlated with a decrease in TRAF3 levels, and nonstructural protein 2 (NS2) has been shown to interact with RIG-I and its expression to correlate with decreases in TRAF3 and STAT2 levels (2, 27).

One drawback of many investigations of hRSV induction of the innate immune response to date has been the lack of spatiotemporal information at the level of the single cell. Previous work in this area has provided considerable insight primarily through biochemical assays, but these investigations often have neglected to study the events of interest within the context of the cell, retaining the spatial organization of hRSV proteins and RNAs. Many representations of the signaling events during hRSV infections depict hRSV genomic viral RNA as randomly distributed throughout the cytoplasm even though this pattern has never been shown via microscopic investigation. Recent time course imaging of hRSV genomic RNA using single-molecule sensitive hybridization probes clearly showed the RNA and the N protein localized near

Received 25 January 2012 Accepted 14 May 2012

Published ahead of print 23 May 2012

Address correspondence to Philip J. Santangelo, philip.santangelo@bme.gatech.edu.

Copyright © 2012, American Society for Microbiology. All Rights Reserved.

doi:10.1128/JVI.00215-12

the plasma membrane in granules of various size during the first 6 h of infection in HEp-2 cells. The pattern progressed to a mixture of smaller granules near the cell membrane and moderate to large inclusion bodies, both at the cell membrane and deeper within the cells, at 12 h postinoculation (14). By 24 hpi, the plasma membrane contained many small granules, filaments, and inclusion bodies, as well as inclusions deeper within the cell. It was observed via subsequent immunofluorescence staining that the N protein colocalized frequently (Manders overlap coefficient, >60%) with the genomic RNA in smaller granules (on the order of the point spread function, ~250 nm) but less frequently in moderate to large inclusion bodies, which often stained around their exterior with anti-N antibodies.

Currently, the function of inclusion bodies in hRSV-infected cells is unknown. It has been speculated that they are sites of replication or transcription, morphogenic intermediates, or sites for the accumulation of dead-end products. Since their earliest mention in the literature, cytoplasmic inclusion bodies have been observed late in hRSV infections using both light and electron microscopy, both in cells infected in culture and in cells from infected children or animals. Inclusions of various size have been immunostained with antibodies to the N, P, M, M2-1, and L proteins, but not for the F or G proteins (5–9), and viral genomic RNA also has been detected either within them or around their perimeter, depending on their size (14, 22). Inclusion bodies have been shown to form spontaneously within cells in culture following the expression of both the N and P proteins, forming inclusions morphologically similar to those observed during viral infections (6). When N or P was expressed separately, inclusions did not form; instead the proteins were distributed evenly throughout the cytoplasm.

Given our previous observations of hRSV organization, our initial goal in the current studies was to couple our previous localization results with additional information regarding the localization of components of the innate immune response such as RIG-I, MDA5, and MAVS, during an hRSV infection. The experiments yielded a number of interesting findings, including data showing that RIG-I and MDA5 colocalized with hRSV granules in the cytoplasm near the plasma membrane as soon as 6 hpi, with MAVS remaining localized to mitochondria. By 12 hpi, MAVS was still partially localized to the mitochondria, but also clearly localized within inclusion bodies, as was MDA5. By 24 hpi, the detectable fraction of MAVS and MDA5 were contained within hRSV granules and inclusion bodies. Given that granules and inclusions can be formed from the coexpression of N and P, we investigated whether the changes in localization observed during the infection occurred with the expression of N and P in the absence of other viral components, and found that the changes in localization still occurred. Next, we postulated that N was interacting with MAVS and MDA5, so we developed a proximity ligation assay (PLA) to assess this interaction *in situ*. PLAs use oligonucleotide-linked antibodies, distance-dependent ligation of DNA to induce circularization, rolling circle amplification, and fluorescently labeled DNA hybridization to test if two proteins interact. The assays can exhibit single interaction sensitivity within a distance of 40 nm (25, 26). Employing such assays we confirmed that N, either expressed alone or simultaneously with the P protein, was in proximity to MAVS and MDA5 *in situ*. It was also found that hRSV N coprecipitated with MDA5 when overexpressed, indicating an interaction, direct or indirect, between the two proteins. Further-

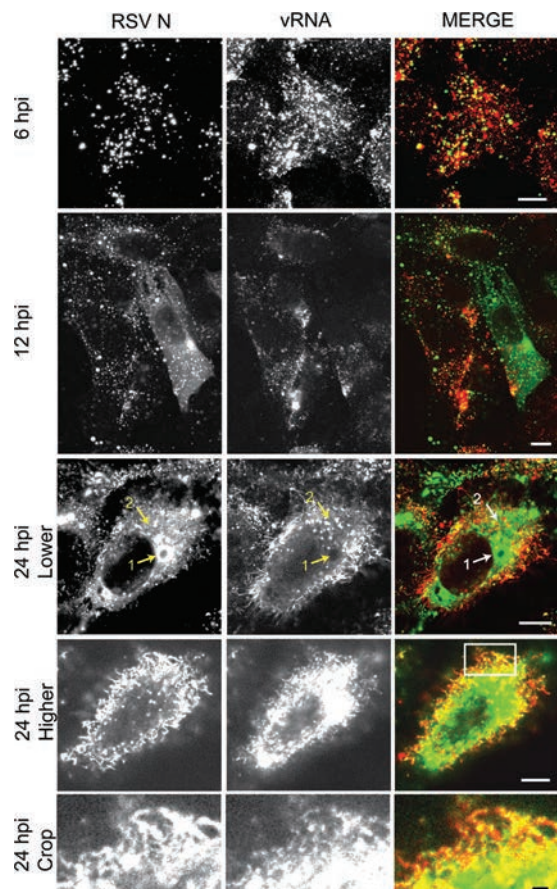


FIG 1 hRSV genomic RNA colocalized with small but not large inclusion bodies (IBs). HEp-2 cells were infected with hRSV strain A2 at an MOI of 1.0 for 6, 12, or 24 h, and subsequently hRSV N was detected using immunostaining and genomic RNA detected with a live cell hybridization probe. Column 1, hRSV N localization. Column 2, localization of viral genomic RNA. Column 3, merge of the first two columns with hRSV N staining in green and genomic RNA in red. Arrow 1, large IB containing hRSV N but not genomic RNA. Arrow 2, region containing small IBs and hRSV N colocalized with genomic RNA. A higher and lower optical plane of the cell at the 24-hpi time point is shown. A crop of the higher plane is shown to emphasize detail of the viral filaments. Scale bars, 10 μ m (top 4 rows) and 5 μ m (row 5).

more, in order to confirm the function of the sequestration of these proteins within inclusion bodies, N and P were coexpressed, and the cells were subsequently infected with Newcastle disease virus (NDV) (LaSota strain). These experiments showed a significant decrease in interferon β mRNA production compared to that during the wild-type infection, giving credence to the function of inclusion bodies as inhibitors of the innate immune response.

Overall, through an examination of the spatiotemporal changes in the localization of proteins involved in the innate immune response, we identified for the first time that the hRSV N protein and subsequent inclusion body formation serve to antagonize the innate immune response likely by interacting with and localizing MDA5 and MAVS.

MATERIALS AND METHODS

MTRIPs. Multiply labeled tetraivalent imaging probes (MTRIPs) were prepared as previously described (23). Briefly, 2'-O-methyl RNA/DNA

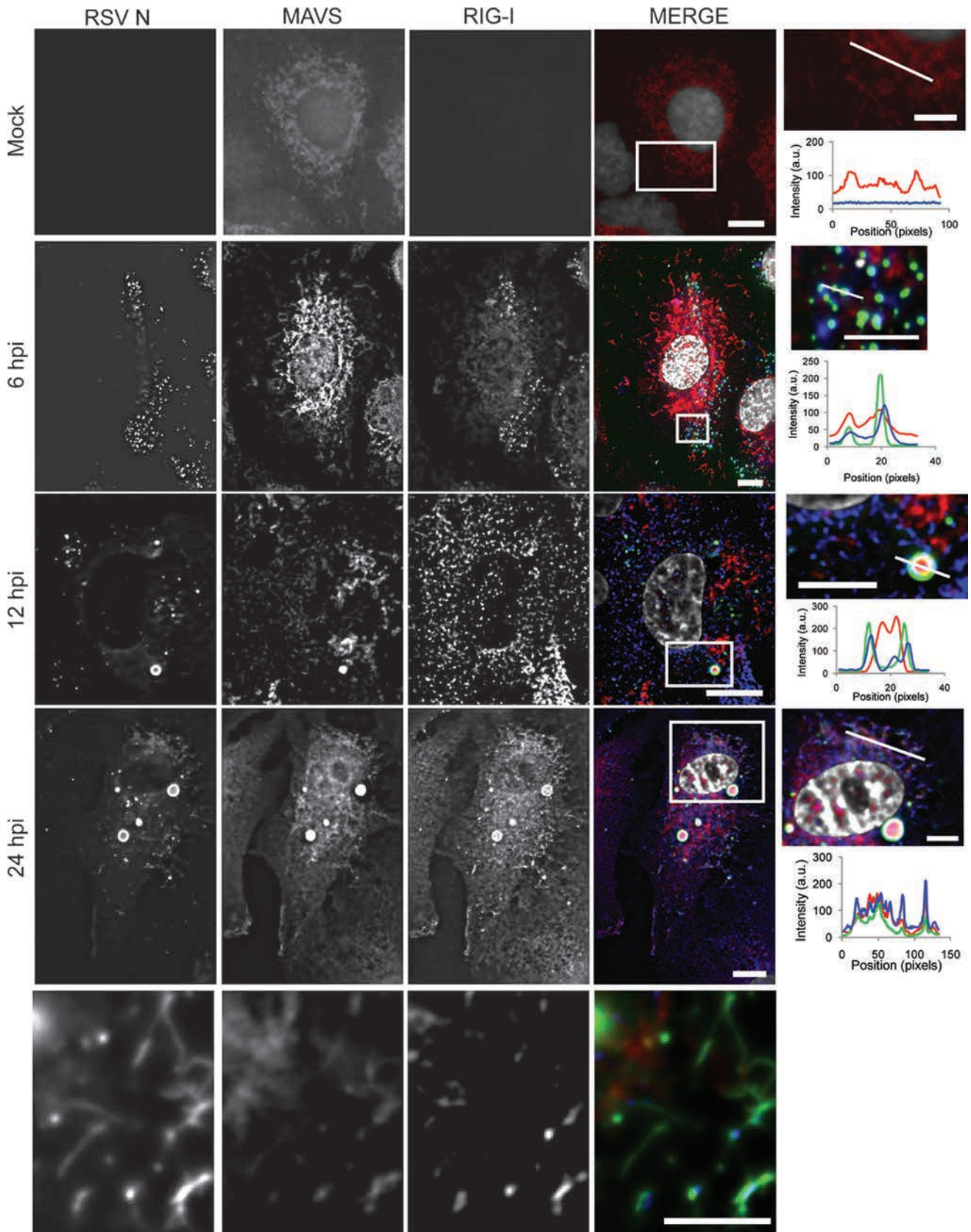


FIG 2 hRSV IBs colocalize with MAVS and RIG-I. A549 cells were infected with RSV strain A2 at an MOI of 1.0 and incubated for 6, 12, or 24 h or were mock infected. hRSV N, MAVS, and RIG-I were detected by immunofluorescence. Column 1, RSV N staining; column 2, MAVS staining; column 3, RIG-I staining. Column 4, merge with hRSV N colored green, MAVS colored red, and RIG-I colored blue. The nucleus, stained by DAPI, is colored white. Column 5, increased-magnification view of the boxes in the merged images. Below each panel is an intensity line graph showing the intensity of each channel along the line in the cropped image. Detail of filaments in a higher optical plane of the cell at the 24-hpi time point is shown in row 5. Scale bars, 10 μ m (column 4, rows 1 to 4) and 5 μ m (column 5 and row 5). Images for the mock infections are wide-field only due to a computational artifact of deconvolving background without positive signal.

chimeric oligonucleotides were synthesized by Biosearch Technologies, Inc., with the following sequence: 5'-biotin-**UXTXTTXXXXAAAXGGGG****CAAAXAA**-3', where the boldface type denotes 2'-O-methyl RNA, the X denotes a dT-C6-NH₂, and all other bases are DNA. The binding region is underlined. MTRIPs were assembled by first conjugating Cy3B-NHS ester fluorophores (GE Healthcare) to the oligonucleotide amine groups using the manufacturer's protocol. Labeled oligonucleotides were then tetramerized by incubation with Neutravidin (Pierce).

Cell culture and viruses. A549 lung carcinoma cells (American Type Culture Collection [ATCC] CCL-185), HEp-2 cells (ATCC CCL-23), Vero cells (ATCC CCL-81), and HeLa cells (ATCC CCL-2) were maintained in high-glucose Dulbecco modified Eagle medium (DMEM) (Lonza) with 10% fetal bovine serum (FBS) (HyClone), 100 U ml⁻¹ penicillin, and 100 µg ml⁻¹ streptomycin (Invitrogen). The hRSV used was the A2 strain (ATCC VR-1544) prepared in HEp-2 cells at a titer of 1 × 10⁶ PFU ml⁻¹. Virus at a multiplicity of infection (MOI) of 1 was adsorbed to the cells for 1 h at 37°C. Following adsorption, fresh medium was added to the inoculum and the cells were incubated for the indicated times. The Newcastle disease virus (NDV) used was the LaSota strain and was a gift of Claudio L. Afonso, USDA. NDV was adsorbed onto cells at an MOI of 5 for 1 h at 37°C. Following adsorption, fresh medium (DMEM with 5% allantoic fluid) was added to the inoculum and the cells were incubated for the indicated times.

RNA probe delivery. For RNA probe delivery, cells were washed in Dulbecco's phosphate-buffered saline (DPBS) without Ca²⁺ and without Mg²⁺ (Lonza), and then incubated with 0.2 U ml⁻¹ activated streptolysin O (Sigma) in Opti-MEM I medium (Invitrogen) containing 30 nM MTRIP for 10 min at 37°C. The delivery medium was replaced with growth medium for 15 min to restore membrane integrity before fixation. In these experiments HEp-2 cells were used for expedience in comparison to previous studies of hRSV RNA and protein localization.

Immunostaining. Cells were fixed with 4% paraformaldehyde (Electron Microscopy Science) in PBS, permeabilized using 0.2% Triton X-100 (Sigma), and blocked with 5% bovine serum albumin (EMD). Cells then were incubated with primary antibody for 30 min at 37°C, washed three times in PBS, and subsequently incubated with the secondary antibody for 30 min at 37°C. Multiple labeling was done sequentially. Cells then were washed three times in PBS, and nuclei were stained using DAPI (4',6-diamidino-2-phenylindole) (Invitrogen). Cells were mounted on slides using Prolong Gold (Invitrogen).

Antibodies. Primary antibodies used were goat anti-RIG-I (Santa Cruz), rabbit anti-MDA5 (ProSci Inc.), rabbit anti-MAVS (Abcam), mouse anti-hRSV N (Abcam), and mouse anti-hRSV P (clone 3_5). Secondary antibodies used were donkey anti-mouse Alexa Fluor 488 (Invitrogen), donkey anti-rabbit Cy3 (Jackson ImmunoResearch), and donkey anti-goat Cy5 (Jackson ImmunoResearch).

Transfection and mitochondrial staining. Vero and HeLa cells were cultured on glass coverslips in 24-well tissue culture plates for imaging experiments or directly in 6-well tissue culture plates for reverse transcription-PCR (RT-PCR). Vero cells were utilized, as they are a common model system for RSV infection, and HeLa cells were used where the interferon response was measured. Both of these cell lines were used in place of HEp-2 and A549, as the latter cells are less efficiently transfected. Cells were transfected using Lipofectamine 2000 (Invitrogen) by the manufacturer's protocol. For each well in the six-well plates, 8 µl of Lipofectamine 2000 and 4 µg of DNA were used. For each well in the 24-well plates, 2 µl of Lipofectamine 2000 and 1 µg of DNA were used. For IB and mitochondria colocalization experiments, Vero cells were grown in glass-bottom petri dishes (In Vitro Sci) and transfected as described above using 2 µl of Lipofectamine 2000 and 1 µg of DNA. Mitotracker 633 was used per the manufacturer's protocols at a dilution of 1:500. Plasmids used were pcDNA3.1, containing optimized cDNAs encoding the RSV A2 strain nucleoprotein (N) and phosphoprotein (P) genes (synthesized by GeneArt, Regensburg, Germany), GFP-MDA5 in a pEGFP-C2 vector (a

gift of Dong-chul Kang), and a GFP-MAVS in a pEGFP vector (a gift of Stanley M. Lemon).

Imaging and processing. Cells were grown on no. 1.5 coverslips and fixed and immunostained. For hRSV N and viral RNA colocalization studies, an LSM 510 confocal microscope (Zeiss) with a Plan-Apochromat primary objective (63×; NA, 1.4) was used. All images were taken using multitrack scanning for each fluorophore to prevent bleed-through. Z-dimension stacks were taken in 0.5-µm increments; the 543-nm laser was used for the Cy3B, the 488-nm laser was used for N protein immunostaining, and the pinholes were set to an Airy unit of 1 (equal in size to an Airy disk). For all other experiments, images were taken on an Axiovert 200 M microscope (Zeiss) with a Plan-Apochromat primary objective (63×; NA, 1.4) and an ORCA-ER AG camera (Hamamatsu). Fluorescent filter sets used were 89000 Sedat Quad - ET for multiple-wavelength imaging (Chroma). All imaging experiments were performed using the Volocity acquisition software (PerkinElmer). Image stacks were recorded at 200-nm intervals for fixed cell samples to adequately sample volumes for iterative deconvolution. Images presented are deconvolved from the wide-field data and linearly contrast enhanced unless otherwise noted. Granule counting and object identification were performed in Volocity. Objects were identified by the standard deviation of intensity and filtered to remove objects less than one point spread function in volume.

qRT-PCR. HeLa cells were grown on six-well plates, transfected as described in the previous section, and inoculated with NDV LaSota strain 24 h posttransfection. Total RNA was extracted at the indicated time points using the RNeasy Minikit (Qiagen). Total RNA was checked subsequently for integrity via agarose gel electrophoresis and quantified via UV-VIS spectroscopy. Total RNA (1 µg) was used for cDNA synthesis using the RT² first-strand kit (SA Biosciences) according to the manufacturer's instructions. A 1-µl portion of the product then was used for quantitative RT-PCR (qRT-PCR) using the real-time RT² qPCR primer assay (SYBR green) in the presence of gene-specific primers for β-actin (ACTB) and beta interferon (IFNB1) (SA Biosciences). qRT-PCR was performed using the ABI StepOnePlus real-time PCR system (Applied Biosciences).

Proximity ligation assays. PLA detection to distinguish between hRSV N or hRSV P protein and MAVS, RIG-I, or MDA5 was performed using the Duolink II kit (Olink Bioscience) with anti-rabbit or anti-goat plus and anti-mouse minus probes according to the manufacturer's protocol. Cells were fixed with 4% paraformaldehyde, permeabilized, and blocked using 0.5% Tween 20 (CalBioChem), 0.1% Triton X-100, 0.1% gelatin (Aurion), 2% donkey serum (VWR), 1% bovine serum albumin in nuclease-free phosphate-buffered saline (PBS). Cells then were incubated with primary mouse anti-hRSV N or mouse anti-hRSV P antibody (1:500) followed by either rabbit anti-MAVS rabbit anti-MDA5 antibody, or goat anti-RIG-I (1:250). Subsequently, cells were incubated with the oligonucleotide-labeled secondary antibodies diluted in 0.05% Tween 20 in nuclease-free PBS.

Spin capture of RSV filaments on glass. In order to capture single hRSV filamentous virions on glass, hRSV A2 was propagated in HEp-2 cells at an MOI of 0.1. At 4 days postinfection the cell-associated and supernatant fractions were scraped, freeze-thawed, and spun through 5-µm- and 0.45-µm-pore-size centrifugal filters (Millipore) at 5,000 × g and 4°C for 4 min and 1 min, respectively. The fraction between 0.45 µm and 5 µm in diameter was collected and spun down onto a poly-L-lysine (Sigma)-coated cover glass at 3,007 × g and 4°C for 30 min. The immobilized virions were fixed using 4% paraformaldehyde and immunostained according to the aforementioned protocol. In addition to the host protein and viral antibodies previously mentioned, virions were also stained with palivizumab, which binds to the hRSV F protein (MedImmune).

Immunoprecipitation and Western blotting. HeLa cells were transfected with green fluorescent protein (GFP)-MAVS and RSV N or GFP-MDA5 and RSV N using Lipofectamine 2000 as described above. Cells were lysed in RIPA buffer (Thermo) supplemented with complete pro-

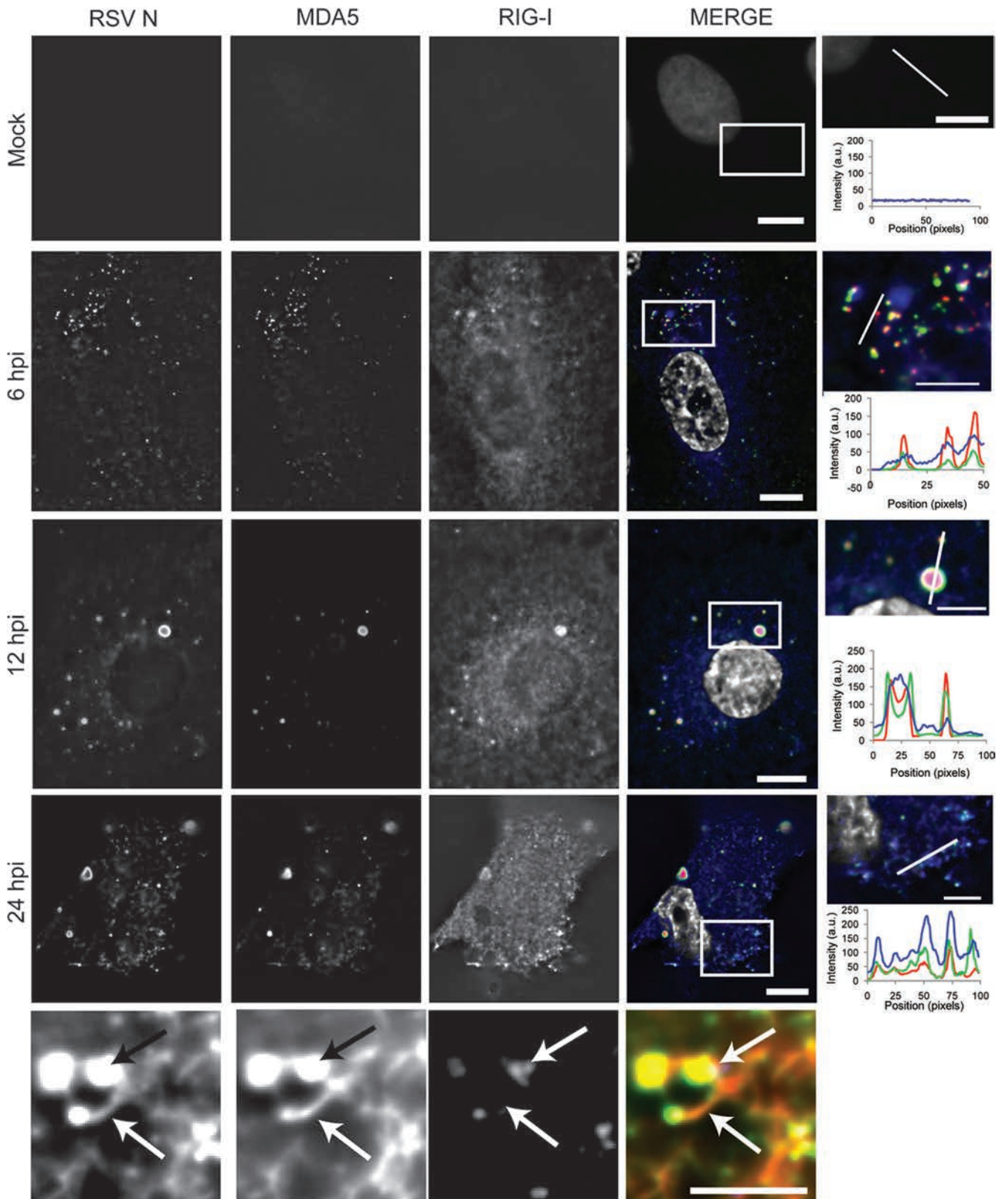


FIG 3 hRSV IBs colocalize with MDA5 and RIG-I. A549 cells were infected with hRSV strain A2 at an MOI of 1.0 and incubated for 6, 12, or 24 h or were mock infected. hRSV N, MDA5, and RIG-I were detected by immunofluorescence. Column 1, hRSV staining; column 2, MDA5 staining; column 3, RIG-I staining. Column 4, merge with hRSV N colored green, MDA5 colored red, and RIG-I colored blue. The nucleus, stained by DAPI, is colored white. Column 5, increased-magnification view of the boxes in the merge image. Below each panel is an intensity line graph showing the intensity of each channel along the line in the cropped image. Detail of filaments in a higher optical plane of the cell at the 24-hpi time point is shown in row 5. The arrows in row 5 point to an inclusion body (upper) and a viral filament (lower). Scale bars, 10 μm (column 4, rows 1 to 4) and 5 μm (column 5 and row 5). Images for the mock infections are wide-field only due to a computational artifact of deconvolving background without positive signal.

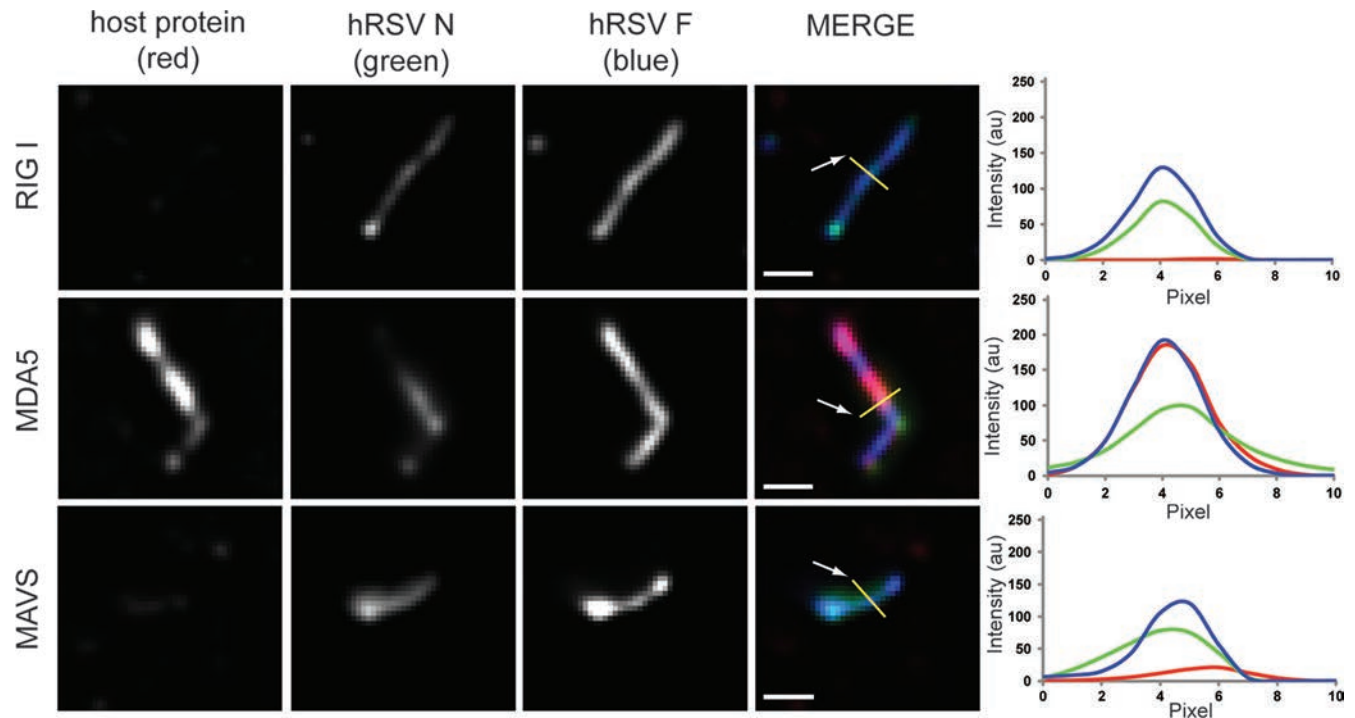


FIG 4 MDA5 colocalized with isolated viral filaments. HEp-2 cells were infected with hRSV strain A2 at an MOI of 0.1, and viral filaments were isolated 4 dpi. Viral filaments were isolated by filtration and adsorbed onto cover glass for immunostaining. Column 1, host protein RIG-I, MDA5, or MAVS, red in the merge. Column 2, hRSV N staining, green in the merge. Column 3, hRSV F staining, blue in the merge. Column 4, merge. Column 5, intensity profile through the lines in the merged images; arrow, pixel number 1. Scale bar, 1 μm .

tease inhibitor (Roche). Lysates were stored at -80°C until use. For immunoprecipitation, Dynabeads coated with sheep anti-rabbit antibodies (Invitrogen) were incubated overnight at 4°C with rabbit anti-GFP antisera (Thermo). The beads were washed, and lysates were added to the beads. Lysates were tumbled overnight at 4°C . The beads were washed to remove unbound proteins. To release the precipitate, SDS buffer (LI-COR Biosciences) was added to the beads and the solution was incubated at 70°C for 10 min. The eluted proteins were loaded into 10% Bis-Tris gels (Invitrogen) and run using MOPS (morpholinepropanesulfonic acid) buffer (Invitrogen). Western transfer was performed in an XCell II blot module (Invitrogen) onto nitrocellulose paper (Invitrogen) according to the manufacturer's protocol. Blotting was performed using a Snap i.d. (Millipore). Blots were blocked using Odyssey blocking buffer (LI-COR Biosciences), and primary antibodies, mouse anti-GFP and mouse anti-RSV N, were diluted in Odyssey blocking buffer with 0.1% Tween 20 (CalBioChem) and incubated on the blots for 10 min. Blots were washed in PBS with 0.1% Tween 20. Secondary goat anti-mouse antibody labeled with DyLight 680B (Thermo), diluted as described above, was incubated for 10 min. Blots were washed as described above. Blots were imaged on an Odyssey (LI-COR Biosciences) at $42\ \mu\text{m}\ \text{pixel}^{-1}$ using the "high" quality setting. Blots were linearly contrast enhanced in ImageJ for clarity. Bands corresponding to RSV N and the GFP-MAVS and GFP-MDA5 were differentially enhanced due to the sensitivity differences of the primary antibodies against the respective proteins.

RESULTS

Localization and structure of granules associated with hRSV N protein and vRNA during infection. We first analyzed the structures and distribution of viral proteins and genomic RNA at 6, 12, or 24 h postinfection (hpi). HEp-2 cell monolayers were inoculated with hRSV strain A2 at an MOI of 1 and incubated in growth medium for the indicated times. Multiply labeled tetravalent im-

aging probes (MTRIPs) were delivered into the live cells as described, and they were subsequently fixed and immunostained for hRSV N (Fig. 1). At 6 hpi, both the viral genomic RNA and inclusion bodies (IBs) positive for hRSV N protein were punctate and colocalized (Fig. 1, row 1). Morphologically, the IBs were round, and no filaments were present. The average volume of the IBs at this time point was $0.9\ \mu\text{m}^3$. At 12 hpi, hRSV N staining was seen both as a diffuse population that filled the cytoplasm and as inclusion bodies, which were larger than those detected at 6 hpi (Fig. 1, row 2). These larger inclusion bodies ($>8\ \mu\text{m}^3$, with an average size of $37\ \mu\text{m}^3$) did not contain genomic RNA detectable with probes, unlike those at 6 hpi. The genomic RNA was located predominantly at the plasma membrane and in smaller granules within the cytoplasm. At 24 hpi, N protein could also be detected in viral filaments on the plasma membrane of the cells in addition to the diffuse hRSV N staining and the staining of IBs (Fig. 1, rows 3 to 5). These filaments contained viral genomic RNA, as previously described (14, 22, 29). Notably the larger IBs contained little to no genomic RNA despite containing high levels of the N protein, which binds to the genomic RNA in the virion.

Viral inclusion bodies colocalize with proteins of the innate immune response. To test whether the hRSV IBs contained proteins of the RIG-I-like receptor (RLR) antiviral response pathway, we infected A549 cells and fixed them at 6, 12, or 24 hpi, or prior to infection (mock), and stained them for hRSV N, MAVS, and RIG-I. In the mock-infected cells no RSV N or RIG-I staining was present and MAVS staining appeared to be mitochondrial (Fig. 2, row 1). At 6 hpi, hRSV N was in a punctate pattern and MAVS staining continued to appear filamentous throughout the cyto-

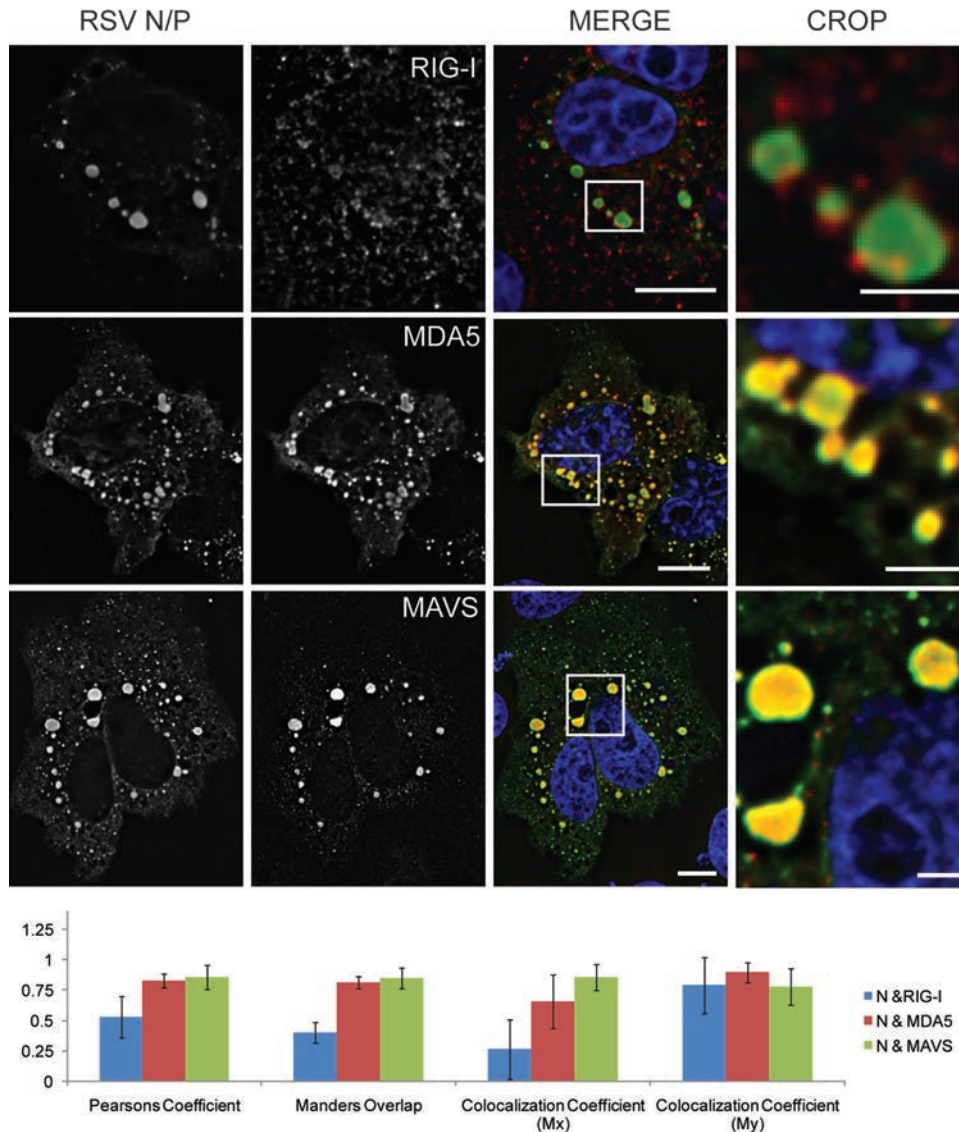


FIG 5 IBs formed by cDNA-based expression of hRSV N and P proteins colocalize with RIG-I, MDA5, and MAVS. Vero cells were transfected with plasmids encoding hRSV N-GFP fusion and hRSV P proteins. Cells were immunostained for N and either RIG-I, MDA5, or MAVS. Column 1, IBs marked by hRSV N-GFP and immunostaining against the N protein. Column 2, immunostaining against RIG-I (row 1), MDA5 (row 2), or MAVS (row 3). Column 3, merge of column 1 (green) with column 2 (red). Nuclei are stained with DAPI and colored blue. Column 4, a higher magnification view of the boxed region of the panels in column 3. The bar graphs show Pearson's coefficient, Manders overlap, and individual components of Manders overlap (Mx and My). Data are from five independent fields. Error bars show standard deviations. Scale bars, 10 μ m (column 3) and 2.5 μ m (column 4).

plasm, indicative of mitochondria, as would be expected (Fig. 2, row 2) (24). RIG-I staining was similar to hRSV N staining and was punctate. All three proteins were present inside the hRSV N IBs, with a strong correlation between the hRSV N staining and the RIG-I staining. At 12 hpi, hRSV N was again in larger IBs that appeared to be hollow (Fig. 2, row 3). MAVS staining at 12 hpi was altered dramatically, with some of the protein localizing to large IBs that were not observed at earlier time points and appeared to be surrounded by a "ring" of hRSV N staining. Cytoplasmic MAVS staining was still present; however, this staining was no longer filamentous and did not resemble mitochondria. RIG-I staining also was increased inside the larger IBs as well as throughout the cytoplasm. At 24 hpi, both MAVS and RIG-I were local-

ized to large IBs and to viral filaments at the plasma membrane (Fig. 2, rows 4 and 5).

In order to see if this change in protein localization was specific to RIG-I/MAVS or was a more general phenomena of the RLR pathway, we next costained for hRSV N, RIG-I, and MDA-5. In the mock-infected cells no RSV N, MDA5, or RIG-I staining was present (Fig. 3, row 1). At 6 hpi, MDA5 was predominately coincident with IBs containing hRSV N, with little cytoplasmic staining apparent outside these regions (Fig. 3, row 2). At 12 hpi, MDA5 colocalized with IBs of all sizes, and there was little to no staining detected outside these regions (Fig. 3, row 3). At 24 hpi, MDA5, like RIG-I, was present in viral filaments at the plasma membrane (Fig. 3, rows 4 and 5).

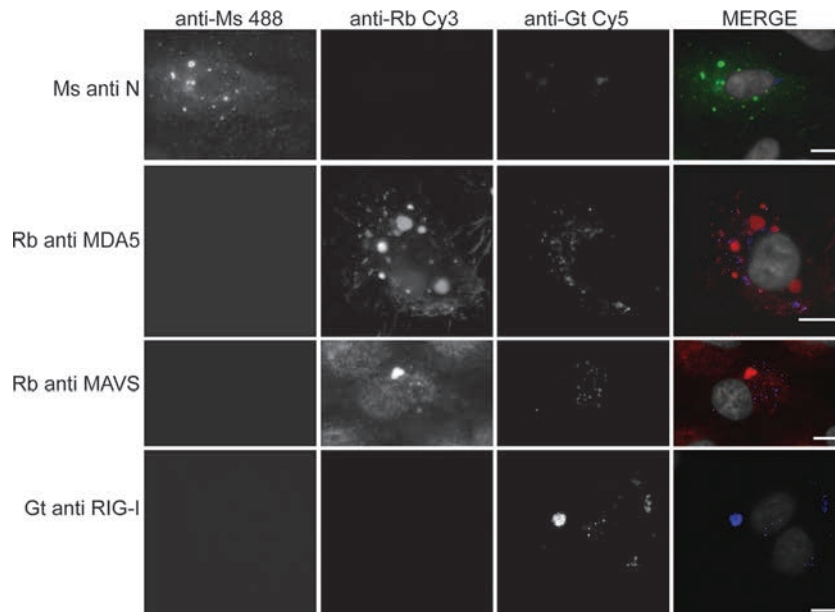


FIG 6 Secondary antibodies do not cross-react with the primary antibodies, nor do the fluorophores bleed through to adjacent fluorescent channels. A549 cells were infected with hRSV strain A2 at an MOI of 1.0 for 24 h and were subjected to immunostaining using a single primary antibody against hRSV N, MDA5, MAVS, or RIG-I. All three secondary antibodies against mouse (Ms), rabbit (Rb), and goat (Gt) were applied. The columns show the individual channels corresponding to the 488-, Cy3-, and Cy5-labeled antibodies and the merge. Scale bars, 10 μ m.

Owing to the dense nature of viral and host proteins near the plasma membrane, it was difficult to separate the bright signal from IBs from the lower signal inside filaments. To circumvent this problem, viral filaments were isolated from infected cells, deposited and fixed on glass coverslips, and immunostained for hRSV F and hRSV N, and RIG-I, MDA5, or MAVS (Fig. 4). While MDA5 stained strongly in the isolated filaments, neither RIG-I nor MAVS was observed to colocalize with them.

Expression of hRSV N and P proteins was sufficient to localize proteins of the innate immune response. In order to test whether the presence of IBs alone was sufficient to localize RIG-I, MDA5, and MAVS, hRSV N and P were expressed in Vero cells that subsequently were fixed and immunostained. As seen in the left column of Fig. 5, the expression of hRSV N and P resulted in the formation of both small and large IB-like structures similar to those seen in the infection model. In these cells, RIG-I staining was increased in and around the IBs; however, RIG-I was not localized exclusively to the IBs. In contrast, both MDA5 and MAVS were localized almost exclusively to the IBs, and little staining was detected outside these regions. In order to quantify these results, colocalization data were obtained from over 100 cells from five fields and were summarized in the graph in Fig. 5. A colocalization analysis between N and RIG-I yielded a Pearson's coefficient of 0.5 and a Manders overlap of 0.4, suggesting the colocalization was strong but not complete. When the Manders overlap was broken into its constitutive parts, Mx and My, it was seen that three-quarters of the N staining colocalized with RIG-I (My, \sim 0.75), while RIG-I staining colocalized with N approximately 25% of the time (Mx, \sim 0.25). In contrast, the Pearson coefficient and Manders overlap for N with MDA5 or MAVS were both $>$ 0.75, and the Mx and My colocalization coefficients in these two cases were both $>$ 0.5, indicating near-complete colocalization between the expressed inclusion bodies and MDA5 and MAVS.

To verify that neither the antibodies were cross-reacting, nor the fluorophores bleeding through to adjacent channels, cells infected with RSV for 24 h were stained with a single primary antibody and all three secondary antibodies, anti-mouse Alexa Fluor 488, donkey anti-rabbit Cy3, and donkey anti-goat Cy5 (Fig. 6). Signal was present only in the correct channel for the primary-secondary antibody combination, indicating that bleed-through of signal from particularly intense staining, such as RSV N, was not occurring at the exposure times used, nor was the cross-reaction of the secondary antibodies leading to detectable signal. There was more background in the Cy5 channel; however, the background was not due to bleed-through or cross-reaction, as both of those would lead to the appearance of IBs in the Cy5 channel coincident with those in the Cy3 or 488 channels, and this result was not observed.

hRSV N is in close proximity to MDA5 and MAVS *in situ*. The colocalization analysis discussed above suggested an interaction between the proteins of the innate immune response and the viral inclusion bodies. However, owing to the limited spatial resolution of the light microscope (\sim 250 nm), a separate assay was needed to demonstrate that the proteins were in close proximity ($<$ 30 nm) and likely interacting in the cell. Immunoprecipitation is commonly used to demonstrate that two or more proteins interact; however, it is fundamentally an *in vitro* assay. The localization of interactions *in situ* is lost and rearrangements of proteins postlysis may interfere with the interpretation of the results. In order to avoid these complications, we employed a proximity ligation assay (PLA) to demonstrate the close proximity of N with MAVS and MDA5 *in situ* during viral infection. Figure 7 shows Vero cells stained for hRSV P (to identify hRSV IBs) and PLA between N and MAVS or MDA5 at 6 and 24 hpi. PLA control experiments can be seen in Fig. 8. At 6 hpi, hRSV P staining resembled the IB granules marked by hRSV N, and the PLA signal between N and MDA5 had

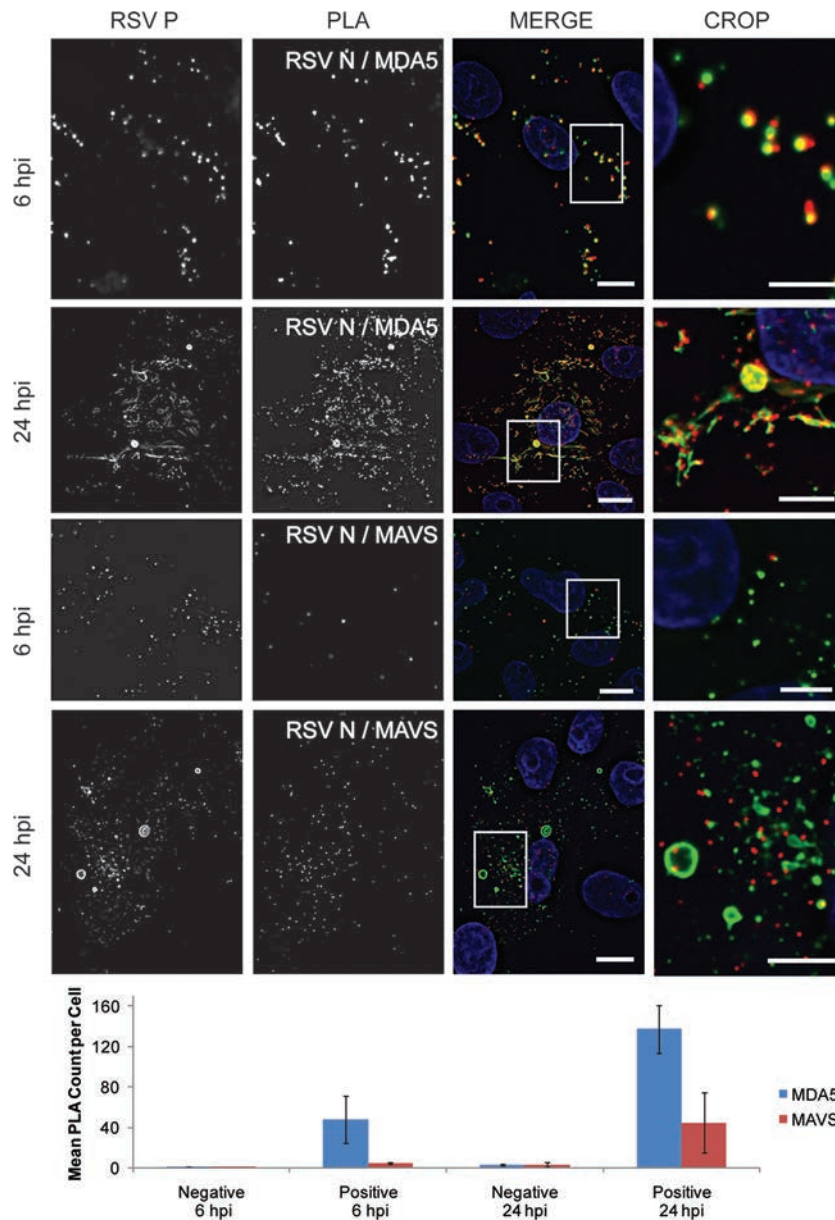


FIG 7 hRSV N interacts with MDA5 and MAVS. Vero cells were infected with hRSV strain A2 at an MOI of 1.0 and incubated for 6 or 24 h. Cells were stained for hRSV P and were assayed for the interaction between hRSV N and either MDA5 or MAVS by PLA. Column 1, immunostaining for hRSV P. Column 2, PLA signal from either hRSV N-MDA5 assays (rows 1 and 2) or hRSV N-MAVS assays (rows 3 and 4). Column 3, merge of column 1 (green) and column 2 (red), with the nucleus stained with DAPI in blue. Column 4, magnification of the boxed region in the panels in column 3. The bar graph shows the mean number of PLA spots per cell detected for each experimental condition along with those for the negative controls (Fig. 8). Error bars are standard deviations. Scale bars, 10 μ m (column 3) and 5 μ m (column 4).

a nearly one-to-one correspondence with the signal from the hRSV P. At 24 hpi, hRSV P staining showed both IB and filamentous structures. The PLA signal between hRSV N and MDA5 at this time point was significantly stronger and, while it is much more heterogeneous than at 6 hpi, there was still a strong correlation between the IBs and filaments with the PLA signal. When PLA was performed between hRSV N and MAVS, there were fewer PLA granules observed. At 24 hpi, this increased; however, it never reached the levels of that of hRSV N/MDA5, and the colocalization between the PLA and hRSV P staining was lower.

hRSV N is in close proximity to MAVS and MDA5 but not RIG-I in the absence of viral infection. To test whether viral replication was required for the interaction between hRSV N and the proteins of the RLR response, PLA was performed between hRSV N and MAVS or MDA5 or RIG-I in Vero cells expressing hRSV N-GFP and hRSV P or only hRSV N-GFP (Fig. 9 and controls in Fig. 10). When hRSV N-GFP was expressed alone, a PLA signal was observed with MDA5 and MAVS, indicating that neither an active viral infection nor any other components of the virus were necessary for this reaction (Fig. 9, rows 2 and 3). In contrast, when PLA was performed between hRSV N and RIG-I, no PLA signal

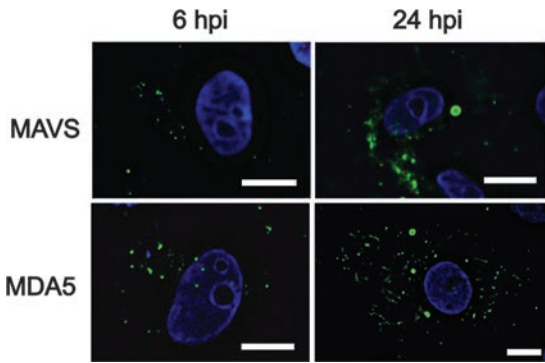


FIG 8 PLA gave no signal in primary antibody control cells infected with RSV. Vero cells were infected with hRSV strain A2 at an MOI of 1.0 and incubated for 6 or 24 h. Cells were stained for RSV P (green) and were assayed for the interaction between RSV N and either MDA5 or MAVS by PLA (red) without the primary antibody for hRSV N. The nucleus, stained by DAPI, is colored blue. Scale bars, 10 μ m.

was observed, indicating that the two were not in close proximity (Fig. 9, row 1). When hRSV N-GFP and hRSV P were coexpressed, the PLA signal was still observed between N and MAVS or MDA5; however, its localization had changed. Instead of being diffuse and cytoplasmic as in the case when hRSV N-GFP was expressed alone, the signal was predominantly around IBs when hRSV N-GFP and hRSV P were coexpressed (Fig. 9, rows 5 and 6). Interestingly, even though RIG-I was present in inclusion bodies when RSV N and P were coexpressed (Fig. 4), it was not in close enough proximity to give a signal from the PLA (Fig. 9, row 4). While MDA5 is soluble and available to bind to targets throughout the cytoplasm, MAVS is localized predominantly to the mitochondria. How MAVS translocated from the mitochondrial surface to IBs is unknown. However, when hRSV N-GFP was coexpressed with the hRSV P and the mitochondria were labeled with MitoTracker, we observed that the mitochondria often surrounded the IBs (Fig. 11). Figure 11A shows a living cell in which the IBs formed from N and P expression were surrounded by mitochondria. To better observe this phenomenon, a 3-D isosurface view was generated (Fig. 11C) from the field in Fig. 11B.

To confirm that RSV N either directly or indirectly interacted as part of a larger complex with MDA5 and MAVS, both GFP-MAVS and GFP-MDA5 were coexpressed with RSV N and were immunoprecipitated using an anti-GFP antibody (Fig. 12). When the precipitates were subjected to Western blotting it was found that N was present in the GFP-MDA5 precipitate but not in the GFP-MAVS fraction (Fig. 12, lanes 1 and 2). No primary antibody controls were negative for the GFP-MDA5, GFP-MAVS, and RSV N proteins (Fig. 12, lanes 3 and 4).

RSV P is in proximity to MDA5 only when coexpressed with RSV N. To test if the proximity of RSV N-GFP and MDA5 and MAVS is unique to RSV N, RSV P-GFP was expressed alone or in combination with RSV N and a PLA was performed between RSV P and MAVS or MDA5. When RSV P-GFP was expressed alone, no PLA signal was observed with either MAVS or MDA5, indicating that overexpression of the viral protein is not sufficient to bring the two into close proximity. When coexpressed with RSV N, PLA signal was observed between RSV P-GFP and MDA5 but not MAVS, indicating that RSV P forms a complex with RSV N that brings it sufficiently close (<30 nm) to MDA5 but not MAVS.

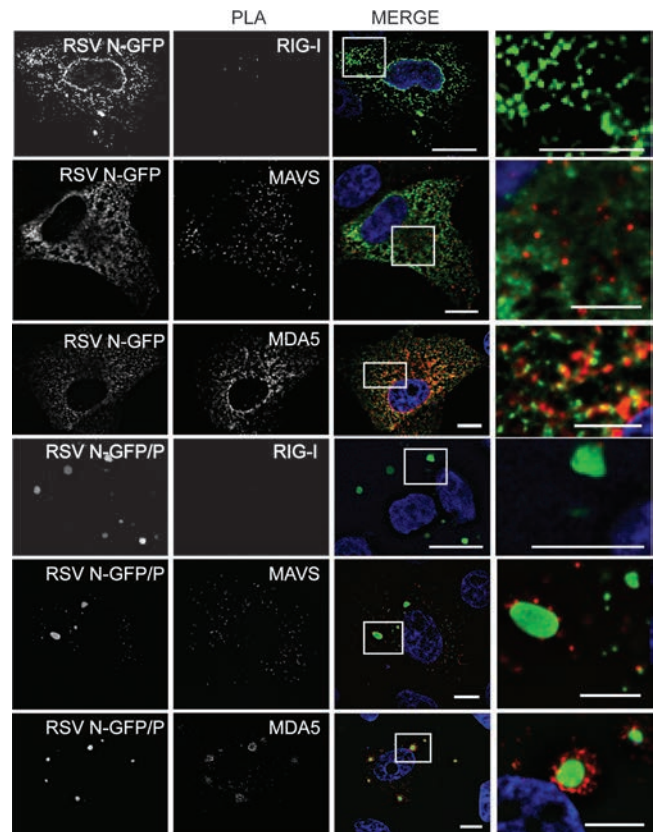


FIG 9 hRSV N is in proximity to MDA5 and MAVS but not RIG-I in the absence of viral infection. Vero cells were transfected with plasmids encoding either hRSV N-GFP or hRSV N-GFP and hRSV P and assayed for the interaction between hRSV N and RIG-I, MDA5, or MAVS. Column 1, GFP signal from the hRSV N-GFP. Column 2, PLA signal for hRSV N with RIG-I (rows 1 and 4), MAVS (rows 2 and 5), or hRSV N with MDA5 (rows 3 and 6). Column 3, merge of column 1 (green) with column 2 (red), with the nucleus stained with DAPI in blue. Column 4, magnification of the boxed region in the panels in column 3. Scale bars, 10 μ m (column 3) and 5 μ m (column 4).

Notably, PLA between RSV P-GFP and MDA5 was exclusively observed around the periphery of IBs. This is in contrast to the PLA between RSV N-GFP and MDA5 or MAVS, which was predominantly but not exclusively localized to IBs (Fig. 13).

To further test if the PLA between RSV N and cellular proteins is an artifact of overexpression of the viral protein, a PLA was performed between RSV N (without the GFP fusion) and a coexpressed GFP control plasmid, which expresses a cytoplasmic, diffusely localized GFP. No PLA signal was observed, indicating that even overexpression of both proteins is insufficient to give a PLA signal if they do not interact. A positive control, RSV N-GFP expression and intramolecular PLA between the RSV N and GFP domains, demonstrated a high level of PLA signal (Fig. 14).

Expression of hRSV N and coexpression of hRSV N and P resulted in the attenuation of interferon response. Given the data presented above, we hypothesized that the interaction of hRSV N with MAVS and MDA5 and the sequestration of these proteins into IBs during infection may cause a decrease in the expression of type 1 interferons and, specifically, interferon β . To test this hypothesis, we transfected HeLa cells with either a GFP control expression plasmid, hRSV N-GFP alone, or hRSV P-GFP alone or cotransfected them with hRSV N-GFP and P. The cells

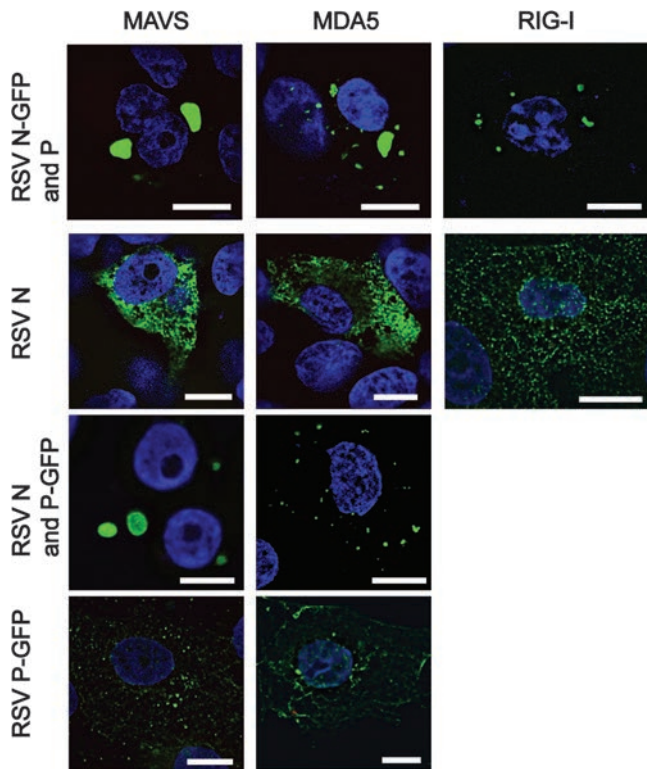


FIG 10 PLA gave no signal in primary antibody control cells transfected with plasmids encoding RSV N-GFP and RSV P, RSV N-GFP alone, RSV P-GFP and RSV N, or RSV P-GFP alone. Vero cells were transfected with plasmids encoding hRSV N-GFP, hRSV N-GFP and hRSV P, hRSV P-GFP, or hRSV P-GFP and hRSV N and assayed for the interaction between hRSV N and MAVS (column 1), MDA5 (column 2), or RIG-I (column 3) without the primary antibody for hRSV N. Row 1, cells transfected with plasmids encoding hRSV N-GFP and hRSV P. Row 2, cells transfected with a plasmid encoding hRSV N-GFP only. Row 3, cells transfected with plasmids encoding hRSV P-GFP and hRSV N. Row 4, cells transfected with a plasmid encoding hRSV P-GFP only. The nucleus, stained by DAPI, is colored blue. Scale bars, 10 μm . Images are single planes of wide-field, undeconvolved Z-stacks.

were subsequently inoculated with the LaSota strain of Newcastle disease virus (NDV), a pathogen known to induce an interferon response through the RLR pathway in HeLa cells (31). At 24 h after NDV inoculation, total RNA was isolated from the cells, and beta interferon (IFNB1) mRNA was quantified relative to β -actin (ACTB) mRNA using reverse transcription real-time PCR

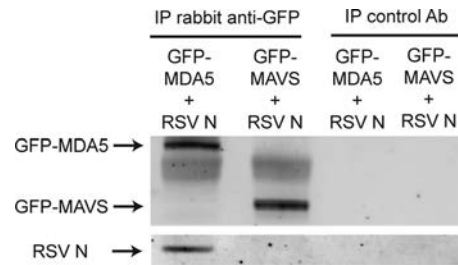


FIG 12 hRSV N coprecipitates with GFP-MDA5. HeLa cells were transfected with plasmids encoding GFP-MDA5 and hRSV N or GFP-MAVS and hRSV N. At 24 h posttransfection, cells were lysed and subjected to IP using an anti-GFP antibody or control antibody. Precipitates were subjected to electrophoresis and Western blotting using an anti-GFP to detect the GFP-MDA5 and GFP-MAVS and an anti-hRSV N antibody to detect the hRSV N. Blots were linearly contrast enhanced.

(Fig. 15). Cells transfected with either hRSV N-GFP or hRSV N-GFP and P and infected with NDV expressed IFNB1 at a level 27 times lower than in cells transfected with GFP control plasmid and infected with NDV (Fig. 15B). When smaller amounts of hRSV N-GFP DNA were transfected into the cells, the effect of hRSV N on interferon expression was diminished in a dose-dependent fashion. In addition, the expression of P alone had no effect on IFNB1 expression, as suggested by the PLA data (Fig. 15B). These data indicated that the effect of hRSV N on the innate immune response lowers the production of IFNB1 when hRSV N is present as a diffuse population throughout the cytoplasm and when it is localized to cytoplasmic IBs.

In untransfected HeLa cells, NDV infection caused IFNB1 expression to increase 150,000-fold at 24 hpi relative to that in uninfected, untransfected HeLa cells. In cells that had been transfected with a GFP control plasmid, NDV infection caused IFNB1 expression to increase 5,000-fold when infected with NDV relative to that in uninfected HeLa cells transfected with GFP. The difference in IFNB1 expression may be due to the transfection process via Lipofectamine 2000. To test if this was the case, cells were treated with the transfection agent alone and infected with NDV. As can be seen in Fig. 15A, the transfection agent, without DNA, reduced the susceptibility of the cells to IFN induction when infected with NDV. While this reduces the overall effect of the sequestration of RLR components on the induction of IFNB1 by NDV in cells expressing hRSV N, there is still a sizable difference (~ 27 -fold) compared to results for cells expressing GFP alone. In

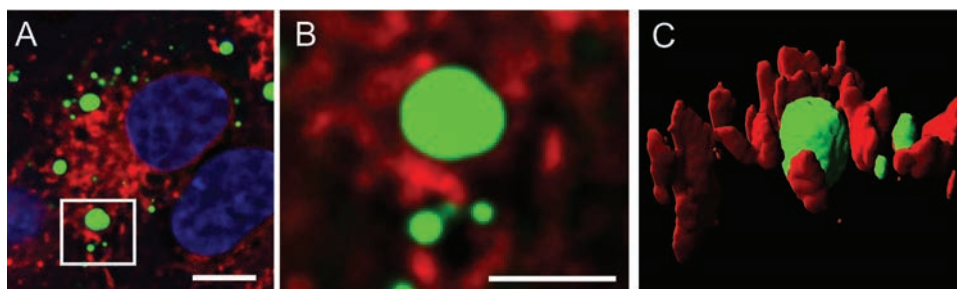


FIG 11 Mitochondria are found adjacent to hRSV IBs. Vero cells were transfected with plasmids encoding hRSV N-GFP and RSV P. At 24 h posttransfection, mitochondria were labeled with Mitotracker deep red 633 and imaged live. (A) Single cell. (B) Magnification of the boxed region in panel A. (C) Three-dimensional isosurface view of a large IB from panel B surrounded by mitochondria. hRSV N-GFP is colored green, Mitotracker is colored in red, and nuclei stained by DAPI are in blue. Scale bar, 10 μm (A) and 5 μm (B).

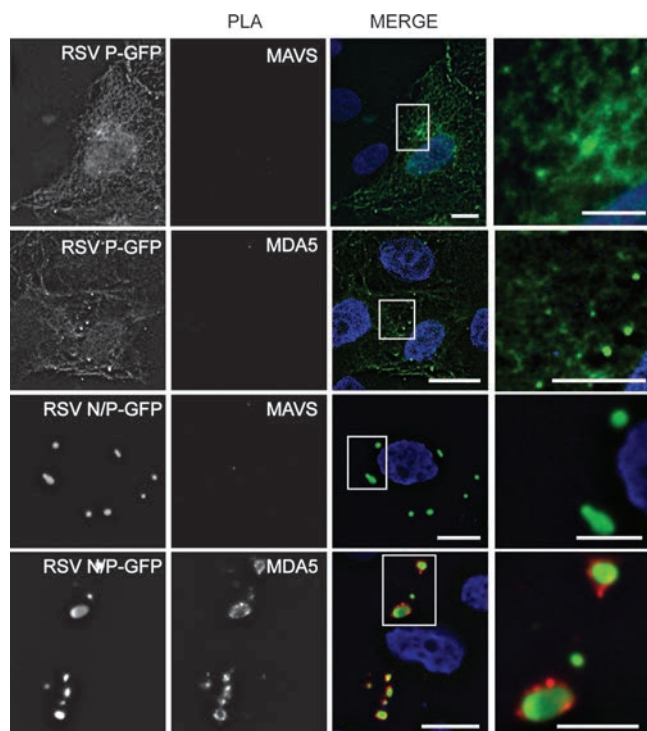


FIG 13 hRSV P is in proximity to MDA5 and MAVS in the absence of viral infection. Vero cells were transfected with plasmids encoding either hRSV P-GFP or hRSV P-GFP and hRSV N and assayed for the interaction between hRSV P and MDA5 or MAVS. Column 1, GFP signal from the hRSV P-GFP. Column 2, PLA signal for hRSV P with MAVS (rows 1 and 3) or hRSV N with MDA5 (rows 2 and 4). Column 3, merge of column 1 (green) with column 2 (red) with the nucleus stained with DAPI in blue. Column 4, magnification of the boxed region in the panels in column 3. Scale bars, 10 μm (column 3) and 5 μm (column 4).

cells transfected with GFP alone, NDV infection caused IFN β 1 expression to increase 27,000-fold relative to the amount in control HeLa cells (no transfection, no infection) and 5,000-fold relative to that in cells that were transfected with GFP and infected with NDV.

DISCUSSION

The experiments presented here demonstrate that one function of the large hRSV inclusion bodies might be to modulate the innate immune response to infection. Although previous experiments have implicated the nonstructural hRSV proteins NS1 and NS2 as modulators of the innate immune response, we demonstrated here that the N protein itself may be involved in that process (3, 4, 15). We studied the role of hRSV N and IBs in modulating the RLR-induced interferon response by colocalization analysis, proximity ligation assay, and immunoprecipitation and by a bioassay using an infection with Newcastle disease virus. We determined that RIG-I, MDA5, and MAVS colocalized with small and large hRSV IBs and that MDA5 and MAVS localized with hRSV N both inside IBs and when expressed diffusely within the cytoplasm. Furthermore, we demonstrated that hRSV N, both expressed diffusely and in IBs, significantly attenuated the interferon response induced by Newcastle disease virus infection in a dose-dependent fashion.

Cytoplasmic IBs, first observed by transmission electron mi-

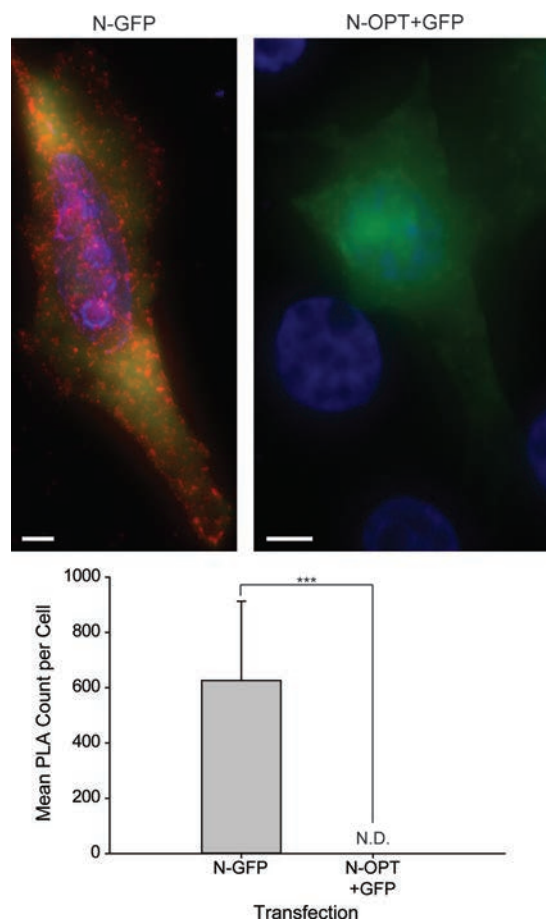


FIG 14 PLA produces a signal in the presence of interacting antigens but not in diffusely localized, noninteracting antigens. Vero cells were transfected with plasmids encoding either hRSV N and free GFP (N-OPT + GFP) or hRSV N-GFP alone (N-GFP). A PLA was performed against the GFP and hRSV N domains in both cases. PLA signal was quantified on a per-cell basis and summarized. Nuclei were stained with DAPI. ***, $P \leq 0.001$. N.D., not detected. GFP signal is shown in green, PLA signal is shown in red, and DAPI signal is shown in blue. Scale bars, 10 μm . Error bars are standard deviations.

croscopy (TEM), are likely aggregates of N proteins (19, 20). Despite the considerable body of knowledge in the molecular biology of hRSV, little is known about the composition, structure, and function of IBs. Previous studies have examined the viral content of IBs and the viral proteins necessary for their formation. It was found that expression of hRSV proteins N and P is sufficient and necessary for the formation of IB-like structures (6). hRSV proteins M, M2-1, and L, when expressed with N and P, also are localized to IBs, while hRSV G and F, which are translated in the endoplasmic reticulum, do not appear to be present in large inclusion bodies but instead have been shown to interact with viral filaments and small IBs or granules close to the plasma membrane (9).

Current and past studies on the localization of hRSV proteins and genomic RNA have shown the important role of imaging methods in the analysis of viral localization and structure. Even so, there is still little known about the heterogeneity of granules and IBs with respect to time, size, or function. Here we showed that hRSV genomic RNA is predominantly localized to small IBs or granules ($<1.0 \mu\text{m}^3$) throughout the course of infection and to

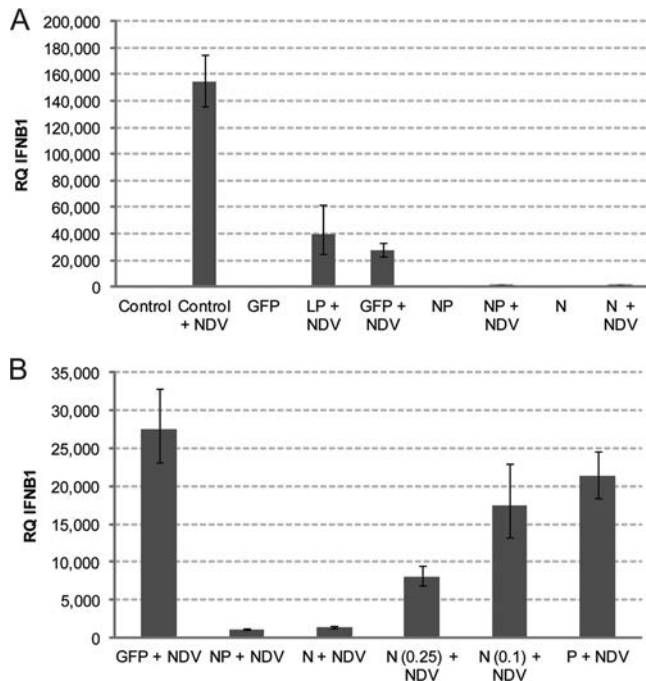


FIG 15 hRSV N expressed alone or with hRSV P functions to diminish interferon expression in response to infection. HeLa cells were either untransfected (control), mock transfected with Lipofectamine 2000 (LP), or transfected with 2 μ g of a GFP-expressing plasmid (GFP), an hRSV N expressing plasmid (N), an hRSV P expressing plasmid (P), or both an hRSV P expressing plasmid and an hRSV N expressing plasmid (NP). After 24 h, cells were left uninfected or were infected with NDV LaSota strain (+ NDV). At 24 h postinfection, cells were harvested for RNA and qRT-PCR was performed for IFNB1 using ACTB as a loading control. (A) Experimental and control cases. (B) Selected data from panel A rescaled, along with hRSV P and a titration of the hRSV N plasmid of one-quarter the amount of DNA (0.25) and one-tenth the amount of DNA (0.1). Error bars are minimum and maximum relative quantification (RQ).

viral filaments during their formation later in the infection (\sim 24 hpi). Contrastingly, even though larger IBs ($>8 \mu\text{m}^3$) contain large quantities of N protein, which is known to complex with viral RNA to form nucleocapsids, they contain little if any genomic RNA, suggesting that this class of IB is likely not the site of viral replication.

By immunofluorescence microscopy, large IBs often are shown to have an open or hollow structure with stronger staining around the periphery of the IB (5, 6, 14). The reason for this structure is unknown, but it is likely an artifact of immunofluorescence, since expressed IBs generated by hRSV N-GFP and hRSV P appear solid

by examination of the GFP signal (Fig. 16); when imaged by TEM, IBs appear solid and uniform (10, 19–21). Given that we have successfully immunostained for proteins within the larger IBs, it is unlikely that the hollow staining pattern is due solely to limited antibody diffusion in fixed IBs. Instead, we propose that this pattern is caused by epitope inaccessibility due to interactions with host proteins. The structure of the N protein-RNA complex of hRSV has been determined; however, the structure of IBs generated by the expression of hRSV N and P has not (28). The structure of IBs, examined in the future at a nanoscale level, may yield clues to the overall functionality of IBs.

Here we suggest that IBs localize proteins of the innate immune response in order to decrease downstream interferon signaling. We demonstrated in a model of hRSV infection that early in the infection, MAVS and MDA5 are localized to small IBs or granules that contain hRSV N and genomic RNA. At later time points, these innate immune molecules are localized to larger IBs that contain little if any genomic RNA and to viral filaments that also contain genomic viral RNA. In both of these cases, the colocalization between the cellular proteins and hRSV N was confirmed by proximity ligation assay (PLA). We further showed that both the colocalization in large IBs and the PLA results were independent of viral infection by expressing hRSV N and P *in trans*, and therefore these findings were not a result of MDA5 interaction with the viral RNA. Finally, we demonstrated, by immunoprecipitation, that hRSV N either directly or indirectly interacted with MDA5. Overall, the picture generated by our data suggests that N interacts with both MDA5 and P within a macromolecular complex. It also suggests that MAVS is a part of this complex, in close proximity to N, but not within 30 to 40 nm of P.

The innate immune response to RNA virus infections proceeds through two pathways, via RIG-I-like helicases, including RIG-I and MDA5, and the TLR pathway. Both of these pathways result in the induction of interferon production. The RIG-I-like proteins require an intermediary protein MAVS (also known as IPS-1, VISA, and Cardif), which binds to RIG-I-like helicases through a caspase activation and recruitment domain (CARD domain). MAVS initiates a signaling cascade by activating cytosolic kinases IKK and TBK1, which then activates transcription factors NF- κ B and IRF3. These transcription factors translocate to the nucleus, where they promote the expression of type I interferons. In hRSV, the interferon response has been shown to play an important role in the nature and severity of the disease (11). MDA5 and RIG-I have both been found to be upregulated in infants infected with hRSV compared to infants that have not been infected.

The finding that MDA5 is efficiently localized into IBs may explain why RIG-I has been shown to have a larger effect on the

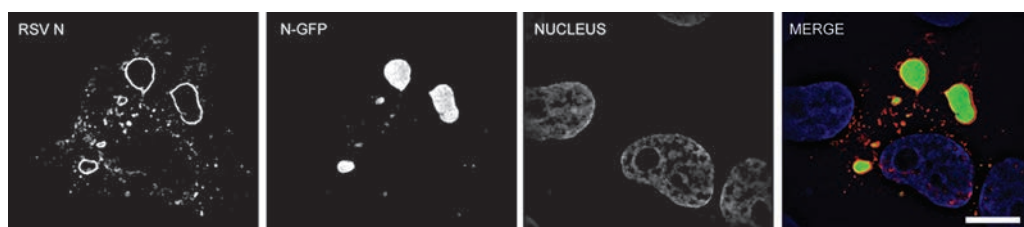


FIG 16 Immunofluorescence staining of expressed IBs yields an open ring-shaped structure. Vero cells were transfected with plasmids expressing hRSV N-GFP fusion and hRSV P proteins and immunostained for hRSV N. The nucleus was stained by DAPI. The merge panel shows the overlay of RSV N immunostaining (red), N-GFP (green), and the nucleus (blue). The image is an XY plane through the center of the largest inclusion bodies. Scale bars, 10 μ m.

innate immune response to hRSV infection (17). The data also suggest a mechanism by which cells can be potentiated toward subsequent infection or coinfection. We have shown that the expression of IBs by hRSV localizes pattern recognition receptors of the RLR pathway and additionally localized their downstream effector MAVS. We demonstrated that N and IBs alone, and not P alone, are enough to diminish the cell's ability to produce interferon in response to a viral infection. To our knowledge, this is the first report of hRSV IBs having a functional role in the life cycle of the virus. It is important to note that while cytoplasmic, diffuse hRSV N expression can decrease the interferon response without the formation of the inclusion bodies, *in vivo* hRSV N is highly localized to IBs (13).

In summary, there are few previous data describing the host cell protein content inside IBs or their precise function. The study presented here suggests an interaction of hRSV N protein with important host proteins of the innate immune response and a specific function for inclusion bodies. The findings also clearly point to the need for further studies regarding IB formation, structure, and function in terms of time and space during hRSV infections.

ACKNOWLEDGMENTS

This work was supported by NIH grant R01GM094198 (P.J.S.) and the March of Dimes (J.E.C.).

In addition, we thank Claudio L. Afonso, ARS, USDA, for the NDV LaSota virus used in this study, Dong-chul Kang, Hallym University, for the GFP-MDA5 vector, and Stanley M. Lemon, University of North Carolina at Chapel Hill, for the GFP-MAVS plasmid.

REFERENCES

- Barbalat R, Ewald SE, Mouchess ML, Barton GM. 2011. Nucleic acid recognition by the innate immune system. *Annu. Rev. Immunol.* **29**:185–214.
- Bitko V, et al. 2007. Nonstructural proteins of respiratory syncytial virus suppress premature apoptosis by an NF-kappaB-dependent, interferon-independent mechanism and facilitate virus growth. *J. Virol.* **81**:1786–1795.
- Bossert B, Conzelmann KK. 2002. Respiratory syncytial virus (RSV) nonstructural (NS) proteins as host range determinants: a chimeric bovine RSV with NS genes from human RSV is attenuated in interferon-competent bovine cells. *J. Virol.* **76**:4287–4293.
- Bossert B, Marozin S, Conzelmann KK. 2003. Nonstructural proteins NS1 and NS2 of bovine respiratory syncytial virus block activation of interferon regulatory factor 3. *J. Virol.* **77**:8661–8668.
- Carrone C, Simabuco FM, Tamura RE, Farinha Arcieri LE, Ventura AM. 2007. Intracellular localization of human respiratory syncytial virus L protein. *Arch. Virol.* **152**:2259–2263.
- García J, García-Barreno B, Vivo A, Melero JA. 1993. Cytoplasmic inclusions of respiratory syncytial virus-infected cells: formation of inclusion bodies in transfected cells that coexpress the nucleoprotein, the phosphoprotein, and the 22K protein. *Virology* **195**:243–247.
- García-Barreno B, Delgado T, Melero JA. 1996. Identification of protein regions involved in the interaction of human respiratory syncytial virus phosphoprotein and nucleoprotein: significance for nucleocapsid assembly and formation of cytoplasmic inclusions. *J. Virol.* **70**:801–808.
- Ghildyal R, et al. 2005. Interaction between the respiratory syncytial virus G glycoprotein cytoplasmic domain and the matrix protein. *J. Gen. Virol.* **86**:1879–1884.
- Ghildyal R, Mills J, Murray M, Vardaxis N, Meanger J. 2002. Respiratory syncytial virus matrix protein associates with nucleocapsids in infected cells. *J. Gen. Virol.* **83**:753–757.
- Jeffree CE, et al. 2007. Ultrastructural analysis of the interaction between F-actin and respiratory syncytial virus during virus assembly. *Virology* **369**:309–323.
- Johnson TR, et al. 2005. Role for innate IFNs in determining respiratory syncytial virus immunopathology. *J. Immunol.* **174**:7234–7241.
- Kurt-Jones EA, et al. 2000. Pattern recognition receptors TLR4 and CD14 mediate response to respiratory syncytial virus. *Nat. Immunol.* **1**:398–401.
- Li D, et al. 2008. Association of respiratory syncytial virus M protein with viral nucleocapsids is mediated by the M2-1 protein. *J. Virol.* **82**:8863–8870.
- Lindquist ME, Lifland AW, Utley TJ, Santangelo PJ, Crowe JE, Jr. 2010. Respiratory syncytial virus induces host RNA stress granules to facilitate viral replication. *J. Virol.* **84**:12274–12284.
- Ling Z, Tran KC, Teng MN. 2009. Human respiratory syncytial virus nonstructural protein NS2 antagonizes the activation of beta interferon transcription by interacting with RIG-I. *J. Virol.* **83**:3734–3742.
- Liu P, et al. 2007. Retinoic acid-inducible gene I mediates early antiviral response and Toll-like receptor 3 expression in respiratory syncytial virus-infected airway epithelial cells. *J. Virol.* **81**:1401–1411.
- Loo YM, et al. 2008. Distinct RIG-I and MDA5 signaling by RNA viruses in innate immunity. *J. Virol.* **82**:335–345.
- Mogensen TH. 2009. Pathogen recognition and inflammatory signaling in innate immune defenses. *Clin. Microbiol. Rev.* **22**:240–273.
- Norrry E, Marusyk H, Orvell C. 1970. Morphogenesis of respiratory syncytial virus in a green monkey kidney cell line (Vero). *J. Virol.* **6**:237–242.
- Norrry E, Marusyk H, Orvell C. 1970. Ultrastructural studies of the multiplication of RS (respiratory syncytial) virus. *Acta Pathol. Microbiol. Scand. B Microbiol. Immunol.* **78**:268.
- Roberts SR, Compans RW, Wertz GW. 1995. Respiratory syncytial virus matures at the apical surfaces of polarized epithelial cells. *J. Virol.* **69**:2667–2673.
- Santangelo PJ, Bao G. 2007. Dynamics of filamentous viral RNPs prior to egress. *Nucleic Acids Res.* **35**:3602–3611.
- Santangelo PJ, et al. 2009. Single molecule-sensitive probes for imaging RNA in live cells. *Nat. Methods* **6**:347–349.
- Seth RB, Sun L, Ea CK, Chen ZJ. 2005. Identification and characterization of MAVS, a mitochondrial antiviral signaling protein that activates NF-kappaB and IRF 3. *Cell* **122**:669–682.
- Soderberg O, et al. 2006. Direct observation of individual endogenous protein complexes in situ by proximity ligation. *Nat. Methods* **3**:995–1000.
- Soderberg O, et al. 2008. Characterizing proteins and their interactions in cells and tissues using the in situ proximity ligation assay. *Methods* **45**:227–232.
- Swedan S, Andrews J, Majumdar T, Musiyenko A, Barik S. 2011. Multiple functional domains and complexes of the two nonstructural proteins of human respiratory syncytial virus contribute to interferon suppression and cellular location. *J. Virol.* **85**:10090–10100.
- Tawar RG, et al. 2009. Crystal structure of a nucleocapsid-like nucleoprotein-RNA complex of respiratory syncytial virus. *Science* **326**:1279–1283.
- Utley TJ, et al. 2008. Respiratory syncytial virus uses a Vps4-independent budding mechanism controlled by Rab11-FIP2. *Proc. Natl. Acad. Sci. U. S. A.* **105**:10209–10214.
- Yoboua F, Martel A, Duval A, Mukawera E, Grandvaux N. 2010. Respiratory syncytial virus-mediated NF-kappa B p65 phosphorylation at serine 536 is dependent on RIG-I, TRAF6, and IKK beta. *J. Virol.* **84**:7267–7277.
- Yoneyama M, et al. 2004. The RNA helicase RIG-I has an essential function in double-stranded RNA-induced innate antiviral responses. *Nat. Immunol.* **5**:730–737.